Investigation of the tip-over condition and motion strategy for a tracked vehicle with sub-tracks climbing over an obstacle on a slope

Ryosuke Yajima[1] and Keiji Nagatani[2]

***Abstract*— Unmanned exploration by robots for volcanic environments has been required. A tracked vehicle is one good candidate. When a tracked vehicle traverses volcanic environment, it faces tip-over because the ground in a volcanic environment is tilted and frequently covered with large rocks and a tracked vehicle climb over such obstacles on a slope. On the other hand, to increase the traversability, various multiple degrees of freedom tracked vehicles equipped with sub-tracks have been proposed. However, the relationship between tip-over condition on a slope and the sub-track's motion has not been sufficiently researched. The primary purposes of this study are to understand the tip-over phenomena for a tracked vehicle with sub-tracks climbing an obstacle on a slope, and to provide the optimal motion strategy. In this paper, the geometric tip-over condition for each sub-track angle and the motion strategy based on the posture at the moment of climbing over were considered. Moreover, experiments were conducted to validate the usefulness of the proposed method. From the results, the derived condition is valid if the robot does not slide down.**

I. INTRODUCTION

Japan has 111 active volcanoes. When an active volcano erupts, various phenomena leading to disasters are caused, e.g., lava flows, pyroclastic flows, and cinders. Therefore, it is highly important to grasp the volcano's situation for disaster prevention and mitigation. However, since active volcanoes are extremely dangerous, the areas around the crater are restricted during its eruption. Therefore, it is difficult for humans to directly survey the volcano. Because of the above background, unmanned exploration by robots has been required, and research and development have proceeded[1][2].

For rapid exploration of a wide area, flying robots, e.g., unmanned aerial vehicles (UAVs), are suitable[3][4][5]. On the other hand, for a detailed exploration of the ground or exploration over a long period, ground-roving robots are useful. However, because the target environments may be rough or have uneven slopes, high traversability is required for the robots. Therefore, a tracked vehicle is one good candidate for a surface-mobile robot that performs volcanic exploration.

The ground in a volcanic environment is frequently covered with large rocks. Tracked vehicles must be able to climb over such obstacles (Fig. 1). However, as the tracked vehicles climb over obstacles, they face the following problems.

[1]Ryosuke Yajima is with the School of Engineering, Tohoku University, 468-1, Aramaki-Aoba, Aoba-ku, Sendai, Miyagi, 980-8579, Japan yajima@frl.mech.tohoku.ac.jp

[2]Keiji Nagatani is with New Industry Creation Hatchery Center, Tohoku University, 6-6-10, Aramaki-Aoba, Aoba-ku, Sendai, Miyagi, 980-8579, Japan keiji@ieee.org

Fig. 1. A tracked vehicle climbing over a rock in a volcanic environment

- **Tipping over** : The robot's center of gravity does not pass over the obstacle, so it tips over backward and lands upside down.
- **Sliding down** : The robot slips off to the bottom.

When a robot tips over, it cannot continue the exploration unless it has a vertically symmetric shape or a mechanism to turn itself over. Some studies have investigated when tracked vehicles tip over while climbing over steps or stairs on flat ground[6][7][8][9][10]. However, a tracked vehicle tipping over while climbing over an obstacle on a slope has not been researched. Therefore, the authors determined the conditions under which a tracked vehicle would tip over while climbing over a circular cross-section obstacle on a slope, and verified the conditions by conducting experiments with fixed and unfixed obstacles[11]. The results revealed the phenomena of a single tracked vehicle tipping over on a slope.

On the other hand, to increase the traversability, various multiple degrees of freedom tracked vehicles equipped with sub-tracks have been proposed[12][13]. Some studies proposed a method of controlling sub-tracks to increase the traversability on uneven terrain[14][15]. However, even in the above studies, the relationship between the specific tip-over condition on a slope and the sub-track's angle has not been sufficiently considered. This relationship must be understood to enable a robot to traverse volcanic environments.

Therefore, in this study, the research objectives are (1) to understand the tip-over phenomena for a tracked vehicle with sub-tracks climbing an obstacle on a slope, and (2) to provide the optimal motion strategy. To simplify the problem, circular cross-section objects were set as target obstacles. The geometric tip-over condition was considered for each sub-track angle, as well as the motion strategy based on the posture at the moment of climbing over. Moreover, experiments were conducted to validate the usefulness of the proposed method. The difference from the previous studies is to deal with slopes and circular obstacles and to analysis

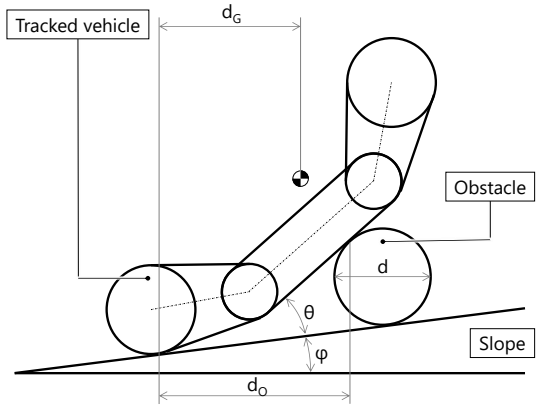

(a) A tracked vehicle with sub-tracks climbing over an obstacle on a slope

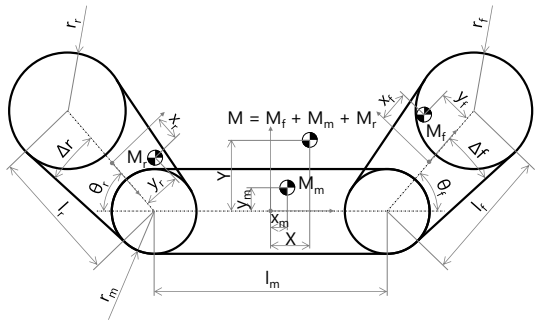

(b) Details of a tracked vehicle: M_m, M_f, M_r are the mass of each tracks, M is the mass of the robot, and the others indicate length or angle of each part

Fig. 2. Assumed model

the tip-over condition for each sub-track's angles in detail.

II. Derivation of the tip-over condition for a tracked vehicle with sub-tracks

A. Research scope

The problems that occur when a tracked vehicle climbs an obstacle are roughly divided into tipping over and sliding down. This research focuses on the former, tipping over, and clarifies the relationship between the sub-track angles and the tipping-over condition.

The target robot is a tracked vehicle with two main tracks and four sub-tracks. The two sub-tracks, front-left and front-right, rear-left and rear-right, are controlled synchronously. Considering volcanic environments, the target environment is not only flat ground but also includes an inclined slope. Although the target obstacle should be complex for realism, an obstacle with a circular cross section is used to simplify the problem. The obstacle is fixed to the ground.

This research considers the condition and motion once the robot has touched the obstacle and begun to climb. In addition, it is assumed that the robot climbs directly from the lower side to the higher side of the slope and the two-dimensional surface of the robot's side view is considered.

B. Geometric tip-over condition of a tracked vehicle with sub-tracks

Rajabi et al. proposed a geometric climbing condition when a tracked vehicle climbs over a step on flat ground[8]. In previous research, we applied this method to a circular cross-section obstacle on a slope, and derived the tip-over condition[11]. In this research, we extend this study and derive the geometric tip-over condition when a tracked vehicle with sub-tracks climbs over a circular cross-section obstacle on a slope.

Fig. 2(a) shows the state when a tracked vehicle with sub-tracks climbs a circular cross-section obstacle on a slope. As described in previous research, the tip-over condition can be derived by the following equations, using the distance d_G, the distance d_O, and the angle θ between the main track and the slope.

$$d_G = d_O \tag{1}$$

$$\frac{dd_G}{d\theta} = \frac{dd_O}{d\theta} \tag{2}$$

This is based on the observation that the robot can climb over the obstacle if its center of gravity reaches just above the contact point between itself and the obstacle. Equation (1) holds when the robot climbs over an obstacle of any diameter. Equation (2) holds when the robot climbs over an obstacle with the maximum diameter that it can climb over. The detailed reason why Equation (2) holds is described in [11]. This condition is the same regardless of whether the robot has sub-tracks.

On the other hand, the distances d_G and d_O are different when the robot has sub-tracks. These are shown by the following equations, using the character in Fig. 2(b).

$$\begin{aligned} d_G = {} & l_r \cos(\theta - \theta_r + \phi) - r_r \sin\phi + \frac{l_m}{2}\cos(\theta + \phi) \\ & + \sqrt{X^2 + Y^2}\cos\left(\theta + \phi + \tan^{-1}\frac{Y}{X}\right) \end{aligned} \tag{3}$$

$$\begin{aligned} d_O = {} & \left\{ l_r \cos(\theta - \theta_r) + r_m \sin\theta - \frac{d}{2}(1 + \cos\theta)\tan\phi \right. \\ & \left. + \frac{\frac{d}{2}(1 + \cos\theta) - r_r - l_r \sin(\theta - \theta_r) + r_m \cos\theta}{\tan\theta} \right\} \cos\phi \end{aligned} \tag{4}$$

The distances d_G and d_O vary according to the sub-track angles θ_f and θ_r. X and Y indicate the position of the robot's center of gravity and are represented by the following equations. These values will vary according to sub-track angles θ_f and θ_r because the sub-tracks also have mass.

$$\begin{aligned} X = {} & \left[M_m x_m + M_f \left\{ \frac{l_m}{2} + \left(\frac{l_f}{2} + x_f \right) \cos\theta_f - y_f \sin\theta_f \right\} \right. \\ & \left. + M_r \left\{ -\frac{l_m}{2} - \left(\frac{l_r}{2} - x_r \right) \cos\theta_r + y_r \sin\theta_r \right\} \right] / M \end{aligned} \tag{5}$$

$$\begin{aligned} Y = {} & \left[M_m y_m + M_f \left\{ \left(\frac{l_f}{2} + x_f \right) \sin\theta_f + y_f \cos\theta_f \right\} \right. \\ & \left. + M_r \left\{ \left(\frac{l_r}{2} - x_r \right) \sin\theta_r + y_r \cos\theta_r \right\} \right] / M \end{aligned} \tag{6}$$

The maximum diameter of an obstacle that a robot with a certain sub-track angle can climb, and the angle θ at the moment when the robot climbs over the obstacle are derived by combining the above equations and solving them simultaneously. By calculating these values for the entire area of the sub-track angles, the tip-over condition on a slope can

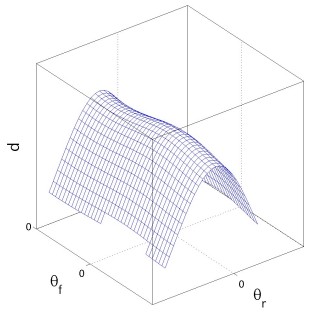

Fig. 3. A tip-over condition (maximum diameter that a robot with a certain sub-track angle can climb)

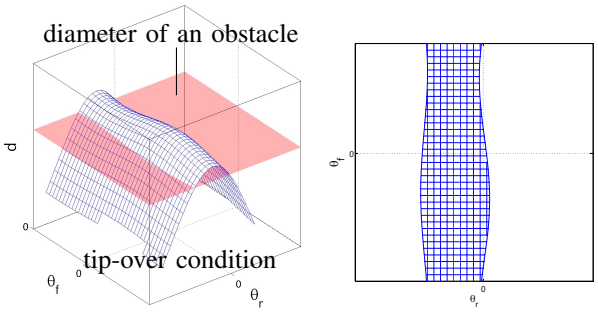

(a) A tip-over condition and a plane surface of the obstacle diameter (b) Area of the sub-track angles that should be chosen

Fig. 4. Posture range for climbing over an obstacle with a certain diameter

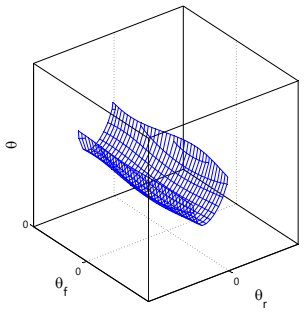

Fig. 5. Angle θ when the robot climbs over an obstacle with a certain diameter

be obtained as a curved surface, e.g., Fig. 3, and the sub-track angle at which the robot can climb over an obstacle with the largest diameter can be found.

III. Motion Strategy Based on the Tip-Over Condition

A. Posture range for climbing over an obstacle with a certain diameter

In Section 2, the maximum diameter of the obstacle that a robot can climb over was derived from the sub-track angles. It is important to understand this for the robot's climbing performance. Practically, however, a robot detects an obstacle in the way, measures the diameter, and then determines the sub-track angle from the diameter.

When a robot climbs over an obstacle with a certain diameter, a sub-track angle should be chosen that will allow the robot to climb over the obstacle. This is visually shown by the curved surface of the tip-over condition and the plane surface of the obstacle diameter; see Fig. 4(a). The area where the curved surface protrudes from the plane surface, i.e., the area in Fig. 4(b), shows the sub-track angles that should be chosen. The boundary of this area can be derived by substituting the obstacle's diameter into the equations in Section 2. If the diameter is less than the maximum diameter, the area of the sub-track angles can be obtained. If the diameter is exactly the maximum diameter, a point of the sub-track angles can be obtained. On the other hand, if the diameter is greater than the maximum diameter, the surfaces do not cross and there is no solution.

B. Optimal posture and motion considered from angle θ at the moment of climbing over

Any sub-track angles in the above area satisfy the geometric condition, and the robot can climb over the obstacle. The difference between each sub-track angle is the size of angle θ at the moment when the robot climbs over the obstacle. Angle θ can be derived from (1), using the obstacle diameter and the sub-track angle. By calculating the entire area, as shown in Fig. 5, a curved surface for angle θ when the robot climbs over the obstacle can be obtained.

Here, considering the situation where the robot climbs over an obstacle, the robot may fall onto its front (at the upper side of the slope) and be jarred by the ground. Considering the safety of the robot, this shock should be as low as possible. Therefore, to reduce the shock, the angle θ at the moment of climbing over should be as low as possible. This is also better from the viewpoint of preventing a slide-down because high-angle θs tend to cause these. According to the above, unless there are specific reasons, the optimal posture is the sub-track angle at which angle θ is the lowest, i.e., the location of the lowest point in Fig. 5.

In some cases, the optimal posture for climbing might not be optimal for approaching the obstacle at the beginning of the climb. For example, when the front sub-track angle θ_f is negative, it is difficult to approach some large obstacles. In those cases, it is necessary to rotate the sub-track from the approaching angle to the climbing angle. The rotation should be controlled so the robot does not tip over.

At the moment when a robot with a certain sub-track angle tips over, angle θ can be derived by the following equation. Calculating for the entire area of the sub-track angles, a curved surface of angle θ when the robot will tip over can be obtained.

$$d_G = 0 \tag{7}$$

This is because the robot tips over when its center of gravity reaches just above the contact point between itself and the ground.

IV. Experiment

A. Description of experiment

To verify the validity of the determined tip-over condition, experiments were conducted using an actual robot. In these experiments, an actual tracked vehicle with sub-tracks climbed an obstacle on a slope, and it was observed whether the robot's motion met the condition.

The rescue robot "Kenaf" was used as the experimental robot (Fig. 6(a)). Kenaf is a tracked vehicle with four sub-tracks. Table I shows Kenaf's specifications, e.g., its size, which is necessary for calculating the tip-over condition. The moving speed was set to 0.05 m/s.

The experimental simulated slope consisted of aluminum frames with a plywood board as the slope (Fig. 6(b)). The incline angle ϕ of this slope can be changed. In this

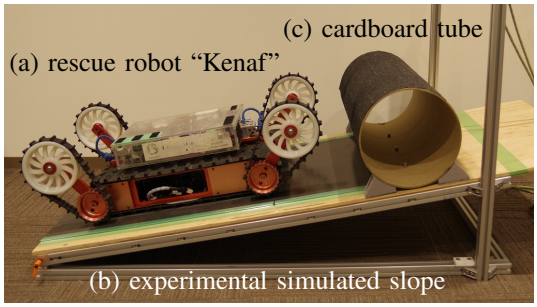

Fig. 6. Experimental equipments

experiment, the incline angle ϕ was set at $0°$ and $10°$. A high-frictional urethane sheet was fastened to the surface of the slope to prevent slipping.

A 260-mm-diameter cardboard tube was used as the obstacle (Fig. 6(c)). This was attached to the slope by bolts. To consider it in two dimensions, the obstacle length was set to 620 mm, which was longer than the width of the robot. Moreover, as with the slope, non-slip tape coated with mineral particles was fastened over the obstacle's surface to prevent slipping.

B. Kenaf's tip-over condition and climbing motion

First, Kenaf's tip-over condition was calculated, based on the method in Section 2, and the results shown in Fig. 7(a) and Fig. 8(a) were obtained. This is the result calculated in $10°$ units of the sub-track angles. Although results can be obtained in which the tracks sink into the ground, because (3) and (4) have conditions allowing the rear sub-track to touch the ground, these results have been omitted. For the $0°$ slope angle, when sub-track angles θ_f and θ_r are set to $-67.11°$ and $-26.91°$, respectively, the robot can climb over the largest obstacle with a 463.03-mm-diameter. For the $10°$ slope angle, when sub-track angles θ_f and θ_r are set to $-67.04°$ and $-36.51°$, respectively, the robot can climb over the largest obstacle with a 397.91-mm-diameter.

Second, the 260-mm-diameter obstacle is considered. Fig. 7(b) and Fig. 8(b) is obtained by cutting the curved surface of the tip-over condition. They indicate the range of the sub-track angle at which the robot can climb over for the $0°$ and $10°$ slope angle. Fig. 7(c) and Fig. 8(c) is obtained by calculating angle θ at the moment of climbing within these ranges, based on the method in Section 3. From these results, for the $0°$ slope angle, when sub-track angles θ_f and θ_r are set to $-16.55°$ and $-73.95°$, respectively, angle θ will be $16.55°$ at the lowest. For the $10°$ slope angle, when sub-track angles θ_f and θ_r are set to $-27.26°$ and $-73.29°$, respectively, angle θ will be $17.26°$ at the lowest.

In this experiment, the initial sub-track angle was set at $\theta_f = \Delta f + 45°$ and $\theta_r = \Delta r + 45°$. The target sub-track angle was set to the following values: (I) the lowest angle θ described above, (II) the sub-track angle at which the bottom of the track is flat ($\theta_f = \Delta f$, $\theta_r = \Delta r$), and (III) the initial sub-track angle ($\theta_f = \Delta f + 45°$, $\theta_r = \Delta r + 45°$). (II) and (III) were chosen for comparison with the optimal condition (I). From the tip-over condition, it is expected that the robot will be able to climb over the obstacle in cases (I) and (II), but not in case (III). The rotation control of the sub-tracks was a constant rotation at a sufficiently high speed. The rotational speed was set at $\pi/12$ rad/s.

TABLE I

PARAMETERS OF KENAF

main track	length	l_m	470 mm
	radius	r_m	47.5 mm
	position of center of gravity	x_m	-13 mm
		y_m	10 mm
	mass	M_m	18.2 kg
front sub-track	length	l_f	155 mm
	radius	r_f	84 mm
	track angle	Δf	13.62°
	position of center of gravity	x_f	16 mm
		y_f	0 mm
	mass	M_f	1.6 kg
rear sub-track	length	l_r	155 mm
	radius	r_r	84 mm
	track angle	Δr	13.62°
	position of center of gravity	x_r	-16 mm
		y_r	0 mm
	mass	M_r	1.6 kg

C. Experimental results for slope angle $\phi = 0°$

Fig. 9 shows the result for the slope with the $0°$ incline angle. The X axis represents the rear sub-track angle θ_r, the Y axis represents the front sub-track angle θ_f, and the Z axis represents the angle θ between the main track and the ground. The mesh curved surface indicates the posture at the moment of climbing over the 260-mm-diameter obstacle. The filled circular mark indicates the initial posture and the filled diamond marks indicate the target postures. Although the curved surface of the posture at the moment of tipping over does not show in this graph (see (7)), the target posture of (III) is on the surface. Each line on the graph shows the changes of the posture, and the marks at the end of the lines show the motion. The circular marks mean that the robot climbed over the obstacle, the x marks mean that the robot tipped over, and the triangular marks mean that the robot slid down. Fig. 10 shows motion of Kenaf. The expected phenomena from the condition and the occurred phenomena in the experiment are summarized in Table II.

As shown in Fig. 9, in cases (I) and (II), angle θ increased gradually with the lifting of the front side of the main track and then decreased gradually because the rear side of the main track was lifted by the rear sub-track. After reaching the target sub-track angle, angle θ increased as the robot advanced, and the robot climbed over the obstacle when it passed the target posture, as expected. On the other hand, in case (III), the robot slid down before reaching the target posture. This is because the friction generated by the sub-tracks was insufficient; the friction required to support the robot increases with the increasing angle θ. Further, when the robot was supported by hand to prevent it sliding down, the robot tipped over at the target posture. Although the experiments were conducted thrice for each case, the results were the same. From the above, the derived condition is valid if the robot does not slide down.

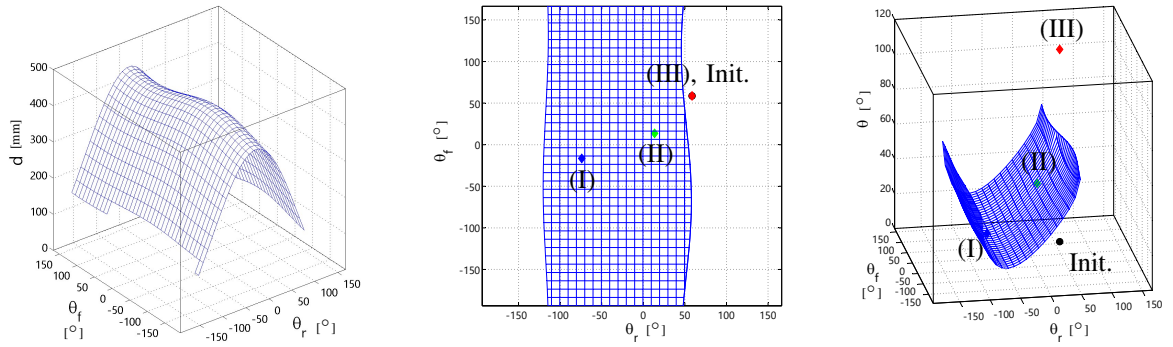

(a) The tip-over condition (the maximum diameter that Kenaf can climb over)

(b) Posture range for climbing over the 260-mm-diameter obstacle

(c) Angle θ when Kenaf climbs over the 260-mm-diameter obstacle

Fig. 7. Kenaf's tip-over condition for the 0° slope angle and the 260-mm-diameter obstacle

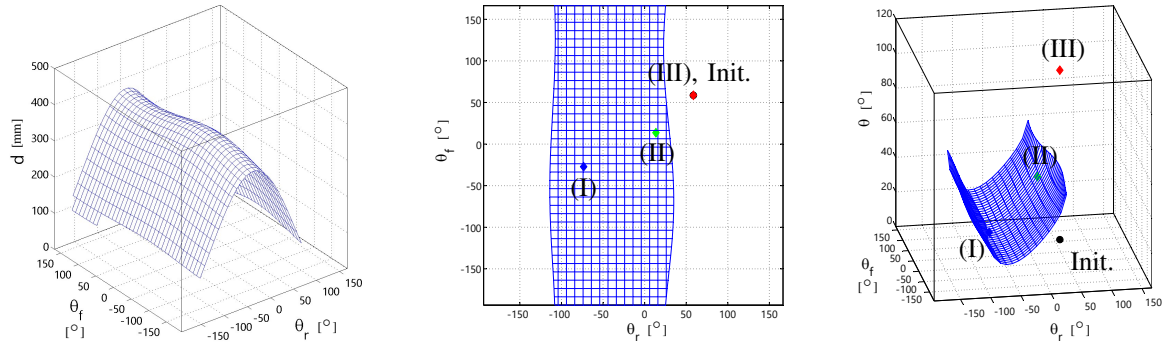

(a) The tip-over condition (the maximum diameter that Kenaf can climb over)

(b) Posture range for climbing over the 260-mm-diameter obstacle

(c) Angle θ when Kenaf climbs over the 260-mm-diameter obstacle

Fig. 8. Kenaf's tip-over condition for the 10° slope angle and the 260-mm-diameter obstacle

D. Experimental results for slope angle $\phi = 10°$

Fig. 11 shows the results for the slope with the 10° incline angle. The meanings of the axes, marks, and lines are the same as in the previous section. Fig. 12 shows motion of Kenaf. The expected phenomena and the occurred phenomena in the experiment are summarized in Table II.

As shown in Fig. 11, in case (I), the robot climbed over the obstacle as expected. On the other hand, in cases (II) and (III), the robot slid down before reaching the target posture because the friction was insufficient. When the robot was supported by hand, it climbed over the obstacle in (II) and tipped over in (III). Although the experiments were conducted thrice for each case, the results were the same. From the above, the derived condition is also valid for the slope if the robot does not slide down. Moreover, by comparing the result of case (I) with the result of case (II), it is suggested that the angle θ for the target posture at the moment of climbing over should be as low as possible to prevent the robot from sliding down. In order to accurately understand this behavior, it is necessary to consider mechanics.

V. CONCLUSIONS

To understand the phenomena that occur when a tracked vehicle with sub-tracks climbs over an obstacle on a slope, and to propose the motion strategy for climbing over, the geometric tip-over condition was derived, the motion strategy was considered, and the results were verified by experiment. When deriving the tip-over condition, the maximum obstacle diameters that the robot could climb over were calculated for each sub-track angle, and a curved surface indicating the tip-over condition was obtained. Considering the motion strategy, given the range of the sub-track angle at which the robot could climb over the obstacle and the posture at which angle θ between the main track and the ground was the lowest within the range, the optimal motion was to rotate the sub-track toward the posture. Moreover, the experimental results confirmed that the robot climbed over or tipped over according to the condition, if it did not slide down.

In future studies, the slide-down condition will be derived, and a more accurate behavior prediction will be realized. The motion strategy from the viewpoint of sliding down and the posture that can be taken from the current posture should be considered. Furthermore, to increase the accuracy, dynamic conditions should be considered. It is also necessary to consider not only fixed obstacles but also unfixed obstacles because unstable rocks in volcanos can be moved by the robots. From a practical viewpoint, some discussion about other shapes and integration with perception systems are required. A safer and more reliable exploration of volcanoes can be realized by extending these studies to three dimensions.

ACKNOWLEDGMENT

We would like to thank Editage (www.editage.jp) for English language editing.

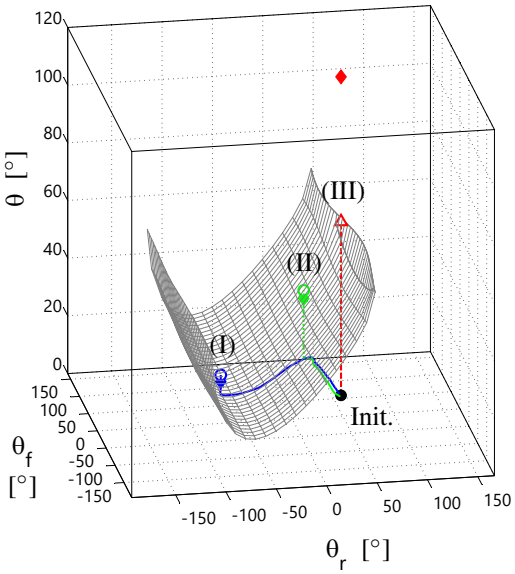

Fig. 9. Changes of sub-track angles and angle θ when Kenaf climbed over the 260-mm-diameter obstacle on the slope with the 0° incline angle

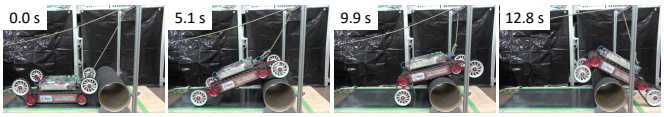

(a) Case (I): Kenaf climbed over the obstacle in 12.8 s

(b) Case (III): Kenaf slid down in 12.8 s

Fig. 10. Motion when Kenaf climbed over the 260-mm-diameter obstacle on the slope with the 0° incline angle

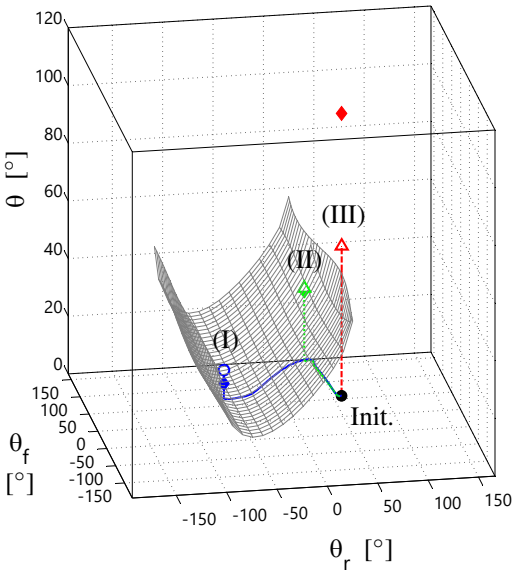

Fig. 11. Changes of sub-track angles and angle θ when Kenaf climbed over the 260-mm-diameter obstacle on the slope with the 10° incline angle

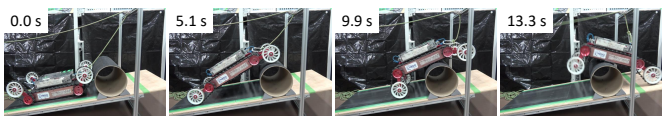

(a) Case (I): Kenaf climbed over the obstacle in 13.3 s

(b) Case (II): Kenaf slid down in 13.1 s

Fig. 12. Motion when Kenaf climbed over the 260-mm-diameter obstacle on the slope with the 10° incline angle

REFERENCES

[1] J. E. Bares and D. S. Wettergreen, Dante II: Technical Description, Results, and Lessons Learned, The International Journal of Robotics Research, vol. 18, no. 7, pp. 621–649, 1999.

[2] K. Nagatani, Review: Recent Trends and Issues of Volcanic Disaster Response with Mobile Robots, Journal of Robotics and Mechatronics, vol. 26, no. 4, pp. 436–441, 2014.

[3] A. Sato, The rmax helicopter uav, Technical report, DTIC Document, 2003.

[4] M. C. L. Patterson, A. Mulligair, J. Douglas, J. Robinson, and J. S. Pallister, Volcano surveillance by ACR silver fox, Proceedings of InfoTech at Aerospace: Advancing Contemporary Aerospace Technologies and Their Integration, pp. 488–494, 2005.

[5] G. Astuti, G. Giudice, D. Longo, C. D. Melita, G. Muscato, and A. Orlando, An overview of the "volcan project": An UAS for exploration of volcanic environments, Journal of Intelligent and Robotic Systems, vol. 54, no. 1–3, pp. 471–494, 2009.

[6] J. Liu, Y. Wang, S. Ma, and B. Li, Analysis of stairs-climbing ability for a tracked reconfigurable modular robot, Proceedings of 2005 IEEE International Workshop on Safety, Security and Rescue Robotics (SSRR 2005), pp. 36–41, 2005.

[7] Y. Liu and G. Liu, Track-stair interaction analysis and online tipover prediction for a self-reconfigurable tracked mobile robot climbing stairs, IEEE/ASME Transactions on Mechatronics, vol. 14, no. 5, pp. 528–538, 2009.

[8] A. H. Rajabi, A. H. Soltanzadeh, A. Alizadeh, and G. Eftekhari, Prediction of obstacle climbing capability for tracked vehicles, Proceedings of 2011 IEEE International Workshop on Safety, Security and Rescue Robotics (SSRR 2011), pp. 128–133, 2011.

[9] W. Tao, Y. Ou, and H. Feng, Research on dynamics and stability in the stairs-climbing of a tracked mobile robot, International Journal of Advanced Robotic Systems, vol. 9, pp. 1–9, 2012.

[10] D. Endo and K. Nagatani, Assessment of a tracked vehicle's ability to traverse stairs, ROBOMECH Journal, vol. 3, pp. 1–13, 2016.

[11] R. Yajima, K. Nagatani, Investigation of tip-over condition for tracked vehicles climbing over an obstacle on a slope, Proceedings of 2017 IEEE/SICE International Symposium on System Integration (SII), pp. 182–187, 2017.

[12] T. Yoshida, E. Koyanagi, S. Tadokoro, K. Yoshida, K. Nagatani, K. Ohno, T. Tsubouchi, S. Maeyama, I. Noda, O. Takizawa, Y. Hada, A High Mobility 6-Crawler Mobile Robot "Kenaf", 4th International Workshop on Synthetic Simulation and Robotics to Miti-gate Earthquake Disaster (SRMED2007), p. 38, 2007.

[13] K. Nagatani, T. Noyori and K. Yoshida, Development of multi-D.O.F. tracked vehicle to traverse weak slope and climb up rough slope, Proceedings of 2013 IEEE/RSJ International Conference on Intelligent Robots and Systems, pp. 2849–2854, 2013.

[14] K. Ohno, S. Tadokoro, E. Koyanagi and T. Yoshida, Semi-autonomous Control System of Rescue Crawler Robot Having Flippers for Getting Over Unknown-Steps, Proceedings of IEEE/RSJInc. Conf.on Intelligent Robots and Systems, pp.3012–3018,2007.

[15] Y. Okada, K. Nagatani, K. Yoshida, Semi-autonomous operation of tracked vehicles on rough terrain using autonomous control of active flippers, Proceedings of IEEE/RSJ International Conference on Intelligent Robots and Systems (IROS 2009), pp. 2815–2820, 2009.

TABLE II

COMPARISON BETWEEN EXPECTATIONS AND EXPERIMENTAL RESULTS

slope angle ϕ		case (I)	case (II)	case (III)
0°	expectation	◯	◯	×
	experiment	◯	◯	△
10°	calculation	◯	◯	×
	expectation	◯	△	△

◯: climbing over, ×:tipping over, △: sliding down